The influence of Ni-rich nanoclusters on the anisotropic magnetic properties of CdSb doped with Ni

2006 Semicond. Sci. Technol. 21 228

(http://iopscience.iop.org/0268-1242/21/3/003)

INSTITUTE OF PHYSICS PUBLISHING SEMICONDUCTOR SCIENCE AND TECHNOLOGY

Semicond. Sci. Technol. **21** (2006) 228–235 doi:10.1088/0268-1242/21/3/003

The influence of Ni-rich nanoclusters on the anisotropic magnetic properties of CdSb doped with Ni

R Laiho[1], A V Lashkul[1,2], K G Lisunov[1,3], E Lähderanta[1,4], I Ojala[1] and V S Zakhvalinskii[1,5]

[1] Wihuri Physical Laboratory, University of Turku, FIN-20014 Turku, Finland
[2] Faculty of Technology, University of Vaasa, FIN-65101 Vaasa, Finland
[3] Institute of Applied Physics, Academiei Str 5, MD-2028 Kishinev, Moldova
[4] Department of Physics, Lappeenranta University of Technology, FIN-53851 Lappeenranta, Finland
[5] Department of Physics, Belgorod State University, RUS-308015 Belgorod, Russia

Received 24 October 2005, in final form 13 December 2005
Published 12 January 2006
Online at stacks.iop.org/SST/21/228

Abstract

The magnetic properties of oriented CdSb single crystals doped with 2 at% of Ni are investigated. From measurements of magnetic irreversibility defined by deviation of the zero-field-cooled (ZFC) susceptibility from the field-cooled (FC) susceptibility, the value of the mean anisotropy field $B_K \sim 4$ kG is obtained. The ZFC susceptibility displays a broad maximum at a blocking temperature, T_b, depending on B according to the law $[T_b(B)/T_b(0)]^{1/2} = 1 - B/B_K$ with $T_b(0) \sim 100$ K. The field dependence of the magnetization exhibits saturation above ~20–30 kG with values of M_s different for B along the [1 0 0], [0 1 0] and [0 0 1] axes. The temperature dependence of M_s is weak, increasing slightly upon cooling the sample below ~100 K. The temperature dependence of the coercive field, $B_c(T)$, is weak above T_b but is enhanced strongly with decreasing temperature below T_b. The anisotropy of B_c is inverted with respect to the anisotropy of M_s. Such behaviour can be attributed to spheroidal Ni-rich $Ni_{1-x}Sb_x$ nanoparticles with a high aspect ratio, broad size distribution and distribution of the orientation of the major axis around a preferred direction. The relation $B_c \ll B_K$ and the anisotropies of M_s and B_c are consistent with reversal of the magnetization by the curling mode, whereas the $T_b(B)$ dependence is typical of the coherent rotation mode. This difference is connected to the proximity of the average transversal cluster radius to a critical value for transition between the two magnetization reversal modes within a wide crossover interval, due to broad distribution of the cluster sizes.

1. Introduction

Interest in the II–V group semiconductor cadmium antimonide, CdSb, having the energy gap $E_g \sim 0.56$ eV and an orthorhombic crystal structure, is connected to its strongly anisotropic transport properties [1] attractive for designing devices as anisotropic thermoelectric sensors [2]. Unintentionally doped (briefly undoped) CdSb is a p-type semiconductor with non-degenerate charge carriers and activated conductivity [1, 3]. Doping of CdSb with different elements influences strongly its transport properties like changing the type of dominating charge carriers from holes to electrons in CdSb:In [1, 4] or inducing a metal–insulator transition and degenerate hole gas in CdSb:Ag [5]. Cyclotron [6] and magnetophonon [7] resonances were investigated in undoped p-CdSb, anisotropic quantum oscillations of the resistivity in p-CdSb:Ag [8] and in n-CdSb:In [9] as well as anomalous anisotropic magnetoresistance due to weak localization of the holes in p-CdSb:Ag [10, 11]. Recently, anisotropic hopping conductivity and complex hole transfer

between the shallow acceptor bands and the valence band maxima were observed in undoped p-CdSb in a strong magnetic field [12, 13].

Undoped CdSb is diamagnetic with different values of magnetic susceptibility $\chi = M/B$ along the crystallographic axes [1 0 0], [0 1 0] and [0 0 1] [1], and contributions of the anisotropy of the lattice and the hole gas to χ have been observed [14]. It was established that the anisotropy of χ in CdSb doped with group I elements did not depend on the kind of impurities but only on their concentration [14, 15]. Fe and Ni substituting for Sb in the lattice were found to act as acceptors [4]. The acceptor impurities Mn and La partially dissolve in CdSb as substitutional impurities forming with Sb a new strongly paramagnetic phase that fully exceeds the diamagnetism of the parent compound [1, 4]. The anomalously large diamagnetic susceptibility found in CdSb crystals doped with Fe was interpreted by formation of impurity clusters [16].

The limited solubility of Ni in the CdSb lattice leads to formation of an eutectic composition CdSb + NiSb at ~2 mol% of NiSb [17]. The microstructure of the eutectic composition consists of needle-like NiSb inclusions of length ~30–40 μm and diameter ~1–1.5 μm in the CdSb host matrix. In addition, the orientation of the needles is distributed around a preferred direction at some angle with the growth direction of the ingot [17]. Therefore, at smaller doping levels of Ni formation of nanosize non-randomly oriented spheroidal Ni-rich $Ni_{1-x}Sb_x$ clusters with a high aspect ratio $m = l/r$, where l and r are the semi-lengths of the major and the minor axes, respectively, can be expected. Because the $Ni_{1-x}Sb_x$ compounds are ferromagnetic at $x \leqslant 7.5\%$ [18, 19], a system of Ni-rich $Ni_{1-x}Sb_x$ nanoclusters in CdSb should exhibit interesting magnetic properties, including blocking of the magnetic moments as typical of an assembly of magnetic nanoparticles and anisotropic features due to large m and preferential orientation of the clusters.

In this work we investigate magnetic properties of CdSb weakly doped with Ni, giving evidence for the presence of Ni-rich $Ni_{1-x}Sb_x$ nanoclusters, and analyse their properties.

2. Experiment

Single crystals of CdSb doped with Ni (2 at%) were prepared by the modified Bridgman method (slow cooling of a melt in the presence of a temperature gradient in the furnace) using a two-stage process. At the first stage Ni was dissolved in Cd annealing the melt at the temperature of 700 °C for 8 h. At the second stage stoichiometric amounts of Sb (purity 99.999%) and Cd:Ni were loaded into a quartz ampoule covered with a thin layer of graphite and filled after evacuation with Ar gas to $p = 0.1$ atm. After keeping the material for 12 h at the temperature of 460 °C the ampoule was cooled down at the rate of 0.5 °C h^{-1}. According to x-ray diffraction the ingots of volume ~1 cm^3 were of single phase material with orthorhombic structure (space group D_{2h}^{15}), and had the same lattice parameters as undoped CdSb. The growth direction of the ingots deviated by an angle of 50° ± 5° from the [1 0 0] crystal axis.

For magnetic measurements, rectangular prisms of dimensions 6.0 × 2.0 × 2.2 mm^3, 6.0 × 1.8 × 2.4 mm^3 and 6.0 × 2.1 × 2.0 mm^3 with the longest edge along the [1 0 0], [0 1 0] and [0 0 1] axes, respectively, were cut from the ingots providing approximately the same angle between each crystallographic axis and the growth direction. The measurements were made with a SQUID magnetometer in fields of $0 \leqslant B \leqslant 6$ T parallel to the crystallographic axes of the three samples defined above. The magnetization $M(T)$ was measured in a field of 50 G–10 kG after cooling the sample from 300 K down to 5 K in zero field (M_{ZFC} or zero-field-cooled magnetization) or in the field of the measurement (M_{FC} or field-cooled magnetization). Thermoremanent magnetization (TRM) was investigated after cooling the sample from the room temperature down to 5 K in a magnetic field and reducing the field to zero.

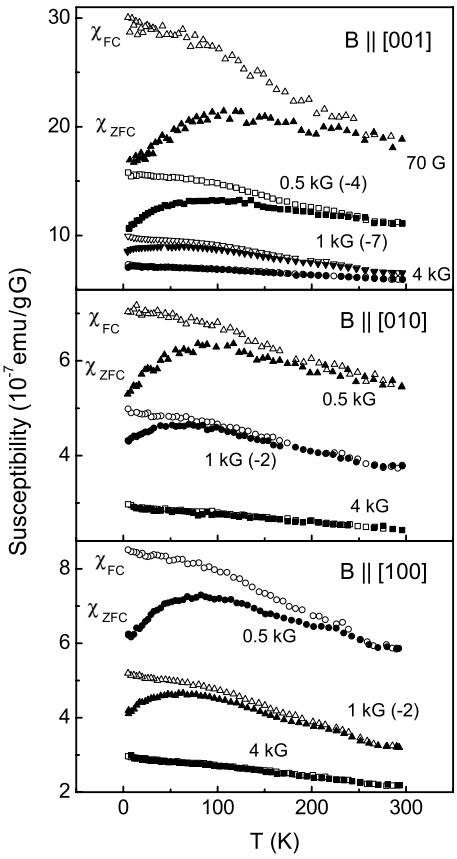

Figure 1. Temperature and magnetic field dependences of χ_{FC} (open symbols) and χ_{ZFC} (closed symbols) of CdSb doped with 2 at% Ni. For convenience some of the curves are shifted along the vertical axis by the values shown in parenthesis in units of 10^{-7} emu g^{-1} G^{-1}.

3. Experimental results

In figure 1 are shown the plots of the magnetic susceptibilities $\chi_{ZFC}(T) = M_{ZFC}(T)/B$ (closed symbols) and $\chi_{FC}(T) = M_{FC}(T)/B$ (open symbols). Here and thereafter the temperature-independent diamagnetic contribution having a linear dependence on B is subtracted from the magnetization data. The magnetic irreversibility or deviation of $\chi_{ZFC}(T)$ from $\chi_{FC}(T)$ in the smallest fields is observed already below 300 K. In addition, $\chi_{ZFC}(T)$ has a broad maximum around

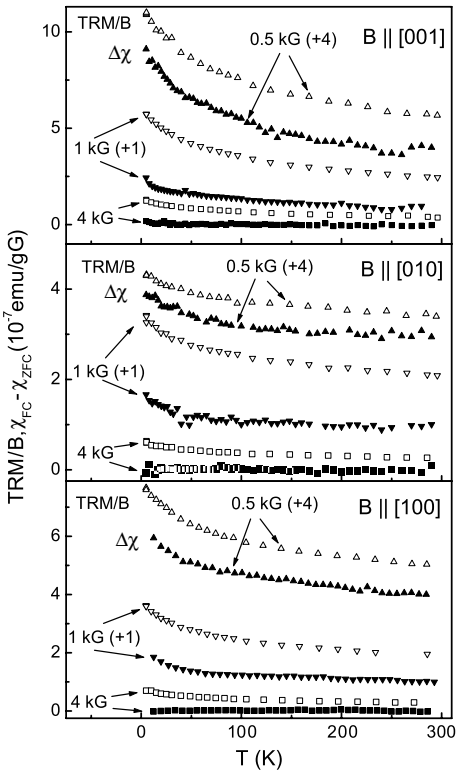

Figure 2. Temperature dependences of TRM/B (open symbols) and $\Delta\chi \equiv \chi_{\rm FC} - \chi_{\rm ZFC}$ (closed symbols) in different magnetic fields. For convenience some of the curves are shifted along the vertical axis by the values shown in parenthesis in units of 10^{-7} emu g^{-1} G^{-1}.

a temperature $T_{\rm b} \sim 100$ K. With increasing B the magnetic irreversibility is damped and becomes unobservable above $B_{\rm K} \sim 4$ kG whereas $T_{\rm b}$ is shifted to lower temperatures. One can also see that for $B \parallel [1\,0\,0]$ and $[0\,1\,0]$ the values of $\chi_{\rm ZFC}(T)$ and $\chi_{\rm FC}(T)$ are comparable and systematically lower than those for $B \parallel [0\,0\,1]$. Also the difference between $\chi_{\rm ZFC}$ and $\chi_{\rm FC}$ decreases with increasing field. The TRM(T) shown in figure 2 (open symbols) follows a similar relation with respect to the crystallographic axes and decreases with temperature. It can also be noted that the temperature dependence of TRM is enhanced when T is decreased and the onset of the enhancement is shifted to a lower temperature when the field is increased.

The field dependence of the magnetization $M(B)$ for each axial direction is similar to that shown in figure 3 for $B \parallel [0\,0\,1]$ (large scattering of the data above ∼1 T is connected to subtraction of the diamagnetic contribution). A rapid saturation of $M(B)$ can be seen already above $B \sim$ 2–3 T. The hysteresis loops show decreasing values of the coercivity and the remanence when T is increased. In figure 4 is shown the saturation magnetization $M_{\rm s}^{(j)}(T)$, the coercivity filed $B_{\rm c}^{(j)}(T)$ and the remanent magnetization $M_{\rm R}^{(j)}(T)$ where $j = 1$, 2 and 3 corresponds to the direction of B along the $[1\,0\,0]$, $[0\,1\,0]$ and $[0\,0\,1]$ axes, respectively. One can see that all of them display the same tendency of enhancement below ∼100 K. In addition, a large difference is observed between the values of $M_{\rm s}^{(1)} < M_{\rm s}^{(2)}$ and $M_{\rm s}^{(3)}$ and the anisotropy of $B_{\rm c}^{(j)}(T)$, $B_{\rm c}^{(1)}(T) > B_{\rm c}^{(2)}(T) > B_{\rm c}^{(3)}(T)$ is inverted with respect to that of $M_{\rm s}^{(j)}$. A non-zero anisotropic

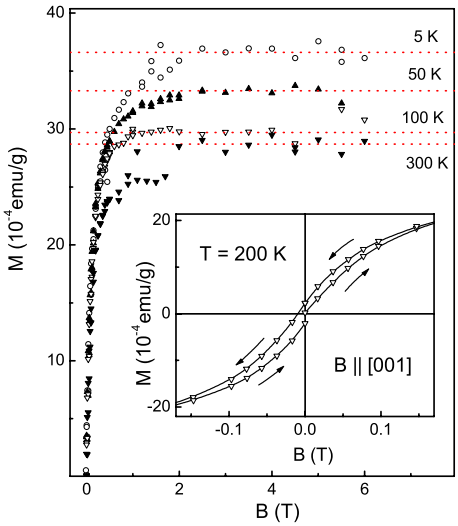

Figure 3. Magnetic field dependence of the magnetization at different temperatures for $B \parallel [0\,0\,1]$. Inset: hysteresis loops measured at $T = 200$ K for $B \parallel [0\,0\,1]$. The dashed lines are to guide the eye.

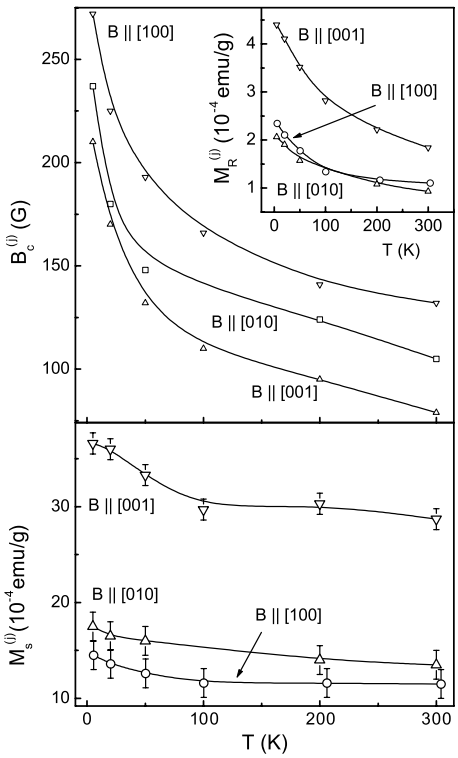

Figure 4. Upper panel: temperature dependences of the coercivity and remanence (inset) for different directions of the magnetic field. Lower panel: temperature dependence of the saturation magnetization for different directions of the magnetic field. The lines are to guide the eye.

coercivity field exists up to 300 K. It is worth mentioning that a weak temperature dependence of the saturation magnetization (as in the bottom panel of figure 4 at $T > 100$ K) persists in our samples at least up to 460 K, which is the highest temperature attainable in our magnetometer.

4. Analysis of the experimental results

The magnetic irreversibility of the samples (figure 1) suggests formation of nanosize magnetic particles. Because at high doping levels the NiSb needles are segregated in the CdSb host, it may be expected that at low doping levels like 2 at% nanoparticles consist of $Ni_{1-x}Sb_x$ which is ferromagnetic at $x \leqslant 7.5\%$ ($T_C = 284$ K at $x = 7.5\%$), with T_C decreasing with increasing x [18, 19]. Since no steep variation of $\chi(T)$, characteristic of a ferromagnetic transition, is observed in our samples up to 460 K, it can be concluded that the Ni-rich nanoclusters are below 460 K in the ferromagnetic state. However, for the nanoparticles this means strong correlations of the internal ion spins due to exchange interaction, but no certain direction of the whole cluster magnetic moment, μ. The moment of a particle can be switched spontaneously between different directions with a frequency $f = f_0 \exp(-KV/kT)$ with $f_0 \sim 10^9$ s^{-1}, provided that the anisotropy energy barrier $\sim KV$, where K is the density of the anisotropy energy and V is the volume of the particle, can be surmounted by the thermal energy kT, which yields to superparamagnetic behaviour. However, with lowering the temperature the thermal excitations $\sim kT$ become insufficient to overcome KV and the spontaneous switching of the moments is transformed into a slow relaxation towards equilibrium or blocking when the moments do not change appreciably during the time of $\tau_e \sim 10^2$ s for static observations [20, 21]. Then the temperature, corresponding to transition from the superparamagnetic to a blocking state, is given by [20]

$$T_b \approx KV/(25\,k). \tag{1}$$

Therefore, the deviation of $\chi_{ZFC}(T)$ from $\chi_{FC}(T)$ and the maximum of $\chi_{ZFC}(T)$ at T_b (figure 1) are attributable to blocking of the moments of the Ni-rich $Ni_{1-x}Sb_x$ clusters. A broad distribution of the sizes of the clusters explains the broadness of the maximum and the large difference between the values of $T_b \sim 100$ K and the onset temperature of the magnetic irreversibility $\sim$300 K observed in weak fields (figure 1). An applied magnetic field reduces the anisotropy energy barriers leading to decreasing of T_b according to an approximate relation

$$[T_b(B)/T_b(0)]^{1/2} = 1 - B/B_K, \tag{2}$$

where B_K is the mean anisotropy field [22]. As $B \to B_K$ the magnetic irreversibility decreases and vanishes for $B \sim B_K$, which explains the damping of the difference between $\chi_{ZFC}(T)$ and $\chi_{FC}(T)$ and shifting of $T_b(B)$ to lower temperatures as may be observed in figure 1. This data yields $B_K \sim 4$ kG. In addition, the values of B_K and $T_b(0)$ are related to the equation $B_K/T_b(0) \approx 2k/\mu(21 + \ln \tau_e)$ [22] which gives at $\tau_e \sim 10^2$ s

$$B_K/T_b(0) \approx 50k_B/\mu. \tag{3}$$

For an assembly of spherical clusters the relation $TRM(T) \approx M_{FC}(T) - M_{ZFC}(T)$ should be fulfilled. Therefore, the large difference between $TRM(T)/B$ (open symbols) and $\chi_{FC}(T) - \chi_{ZFC}(T)$ (closed symbols) in figure 2 suggests a considerable non-sphericity of the Ni-rich clusters [23] in CdSb:Ni. In turn, the large difference of χ_{FC}, χ_{ZFC} and TRM for $B \parallel [1\,0\,0]$ or $[0\,1\,0]$ in contrast with $B \parallel [0\,0\,1]$, suggests non-random orientation of the clusters around a preferred direction.

It should be noted that the above discussion and equations (1)–(3) are valid without restrictions only for an assembly of *single-domain* particles and the magnetization reversal process by *coherent rotation*, when all spins of the ions in the cluster remain parallel to each other. Such a situation takes place when the conditions $r \ll r_{sd}$ and $r \ll r_c$ are fulfilled, where r_{sd} and r_c are the critical radii of a single-domain particle and the coherent rotation, respectively, given by the equations

$$(N_c/6A)(M_s^*)^2 r_{sd}^2 = \ln(4r_{sd}/a) - 1 \quad \text{and}$$
$$r_c = q(2/N_a)^{1/2} A^{1/2}/M_s^*. \tag{4}$$

Here M_s^*, a and A are the zero-temperature saturation magnetization, the mean distance between the magnetic ions and the exchange stiffness constant of the cluster material, respectively, and $N_a(m)$ is the demagnetization factor of the cluster [24, 25]. In the case of spheroidal particles $N_c(m)$ and $N_a(m)$ refer to the major and minor axes, respectively, and are given e.g. in [26]. Another condition is that the intercluster interaction energy $W \ll KV$ is not important for blocking.

As can be seen from the top panel of figure 5 the field dependence of T_b is close to that given by equation (2) for any direction of B without displaying a measurable anisotropy. The parameters $T_b(0)$, B_K and μ, obtained with linear fits of the plots in figure 5 for different orientations of B are the same within the limits of error (see table 1). In addition, the value of μ is typical of a nanosize magnetic particle, whereas that of B_K agrees with the above estimation from vanishing of the magnetic irreversibility with increasing B.

The temperature dependence of the coercivity of an assembly of blocked nanoparticles is given by

$$B_c^{(j)}(T) = B_c^{(j)}(0)\{1 - [T/T_b(0)]^n\}, \qquad j = 1, 2 \text{ and } 3, \tag{5}$$

where $B_c^{(j)}(0)$ and n depend on the magnetization reversal mode [27]. For coherent rotation $n = 1/2$ [21]. For $r_{sd} \gg r \gg r_c$ the magnetization reversal by *curling* would set in. This is connected to the case that the neighbouring spins of the cluster ions are not constrained to be parallel, leading to $n = 2/3$ in equation (5) [27]. Finally, for $r > r_{sd}$ the magnetization reversal by motion of weakly pinned domain walls would yield $n = 1$ [28].

For coherent rotation of an assembly of randomly oriented spheroids, $B_c^{(j)}(0) = \alpha^{(j)} B_K$ with $\alpha^{(j)} = 0.479$ for any j [29]. If there is a preferred orientation, characterized by the angle θ_j between the major axis of a spheroid and the jth crystallographic axis, one has $\alpha^{(j)} = (\cos^{2/3}\theta_j + \sin^{2/3}\theta_j)^{-3/2}$ for $0 < \theta_j < 45^\circ$ and $\alpha^{(j)} = \sin\theta_j \cos\theta_j$ for $45^\circ < \theta_j < 90^\circ$ [26], where the values of θ_j are constrained by the equation

$$\cos^2\theta_1 + \cos^2\theta_2 + \cos^2\theta_3 = 1. \tag{6}$$

As follows from table 1 and the upper panel of figure 4 we have $B_c^{(j)}(T) \ll B_K$ for any j and T. Therefore, the relation $B_c^{(j)}(0) \ll B_K$ should be fulfilled, too, due to the absence of a discontinuity in the function $B_c^{(j)}(T)$ at $T \to 0$ as follows from equation (5). This corresponds to $\alpha^{(j)} \ll 1$. However, it is easy to see that equation (6) and the equations for $\alpha^{(j)}$ above exclude an orientation or a set of θ_j when *all* $\alpha^{(j)}$ *are simultaneously much smaller than unity*. Therefore, independently of the exact value of n in equation (5) it is

Table 1. The values of the zero-field blocking temperature $T_b(0)$, the anisotropy field B_K, the mean cluster moment μ, the zero-temperature values of the coercive field $B_c^{(j)}(0)$, the mean angles $\theta_j^{(B)}$ and $\theta_j^{(M)}$ and the widths of the angular distribution $\Delta_j^{(B)}$ and $\Delta_j^{(M)}$, obtained from the coercivity and the magnetization data, respectively.

Orientation	$T_b(0)$ (K)	B_K (kG)	μ ($10^4\ \mu_B$)	$B_c^{(j)}(0)$ (G)	$\theta_j^{(B)}$ (°)	$\Delta_j^{(B)}$ (°)	$\theta_j^{(M)}$ (°)	$\Delta_j^{(M)}$ (°)
$B \parallel [1\,0\,0]$	107 ± 5	3.9 ± 0.5	2.0 ± 0.2	320	60	3	66	3
$B \parallel [0\,1\,0]$	105 ± 5	4.7 ± 0.5	1.7 ± 0.2	271	54	4	62	5
$B \parallel [0\,0\,1]$	110 ± 3	4.5 ± 0.5	1.8 ± 0.2	244	49	7	39	6

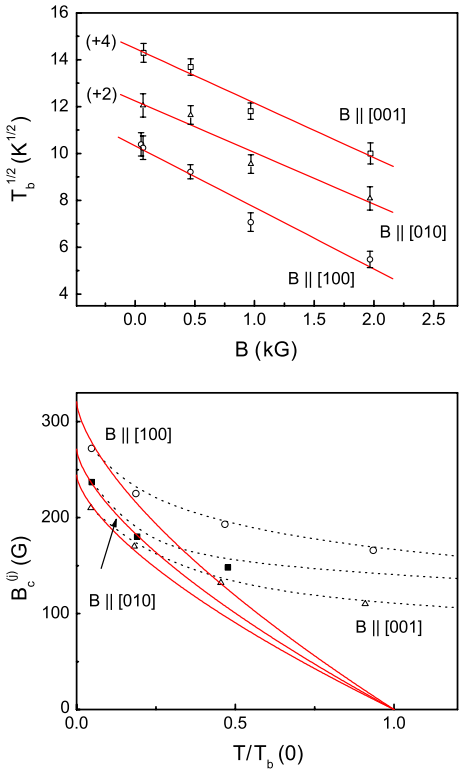

Figure 5. Upper panel: dependence of $T_b^{1/2}$ on the magnetic field for different directions of B. The lines are linear fits. For convenience two plots are shifted along the vertical axis by the values shown in parenthesis in $K^{1/2}$. Lower panel: dependence of $B_c^{(j)}$ on $T/T_b(0)$ for different directions of the magnetic field. The solid lines are calculated with equation (5) and $n = 2/3$ as described in the text, the dotted lines are to guide the eye.

evident that the coercivity in the bottom panel of figure 5 within the blocking regime (i.e. at T definitely below T_b) does not satisfy the conditions of coherent rotation of the moments of single-domain particles.

Our attempts to fit the data of $B_c^{(j)}(T)$ using equation (5) with $n = 1/2$, $2/3$ or 1 were partially successful only within a narrow temperature interval of $T = 5$–20 K. A typical example of the calculations using $n = 2/3$ is shown with the solid lines in the bottom panel of figure 5, which does not allow us to obtain a correct value of n for establishing the origin of the coercivity in this way. An obvious reason for such a situation is the broad distribution of the parameters of Ni-rich clusters in CdSb around their mean values, including the radius, the aspect ratio and the orientation of the spheroids. In particular, this reason is likely to be responsible for the non-zero coercivity of the material even at $T \gg T_b$ (figure 4, top panel). Another reason may be strong intercluster interactions, when equation (5) is not applicable. The role of such interactions in blocking of the cluster moments will be discussed further in section 5.

Next we analyse the coercive field $B_c^{(j)}(0)$, assuming the single-domain model and magnetization reversal by curling. This is useful to do along with the corresponding analysis of $M_s^{(j)}(0)$. For the approximative zero-temperature coercivity data we take the values obtained by fitting of $B_c^{(j)}(T)$ to equation (5) with $n = 2/3$, collected in table 1. For the zero-temperature magnetization we utilize the values at 200 K lying within the interval of weak variation of $M(T)$ as shown in figure 4 (the reason for such a choice will be discussed in section 5). In the case of magnetization reversal by curling we have

$$B_c^j(0) = 2\pi M_s^* \times \frac{(2D_c - \kappa/S^2)(2D_a - \kappa/S^2)}{\sqrt{(2D_c - \kappa/S^2)^2 \sin^2\vartheta_j + (2D_a - \kappa/S^2)^2 \cos^2\vartheta_j}}, \quad j = 1, 2 \text{ and } 3, \tag{7}$$

where $D_a(m) \equiv N_a(m)/(4\pi)$, $D_c(m) \equiv N_c(m)/(4\pi)$, $S = r/r_0$, $r_0 = A^{1/2}/M_s^*$, $\kappa = q^2/\pi$ and q is the smallest solution of the Bessel functions having the limiting values of $q = 1.8412$ for $m \to \infty$ (the infinite cylinder) and $q = 2.0816$ for $m = 1$ (the sphere) [26], whereas the distributions of θ_j, r and m around their mean values are neglected. In this approximation and for a high enough aspect ratio the magnetization of a spheroid is directed close to its major axis and the components of the zero-temperature saturation magnetization can be given as

$$M_s^{(j)}(0) = \eta M_s^*[1 - D(\theta_j)]\cos\theta_j, \quad j = 1, 2 \text{ and } 3, \tag{8}$$

where η is the volume fraction of the $Ni_{1-x}Sb_x$ phase and $D(\theta_j) = D_a \sin^2\theta_j + D_c \cos^2\theta_j$ for a spheroid, satisfying the constraint equation

$$D(\theta_1) + D(\theta_2) + D(\theta_3) = 1. \tag{9}$$

Generally, at arbitrary m the magnetization may not be parallel to the major axis of the spheroid, having an angle φ_j ($j = 1$, 2 and 3 corresponding to different orientations of the field) connected to θ_j with the equations

$$\tan\varphi_j = (X/Y)^{1/2}\tan\theta_j/[(X/Y)^{1/2} + \tan^2\theta_j], \quad j = 1, 2, 3, \tag{10}$$

where $X = (2D_c - \kappa/S^2)^2$ and $Y = (2D_a - \kappa/S^2)^2$.

M_s^* can be excluded with equations (6) and (7) and we find $\cos^2\theta_j = (2X + Y - Z_jX)/[Z_j(Y - X)]$, where $Z_j = \left[B_c^{(j)}(0)\right]^2 \sum_{j=1}^3 \left[B_c^{(j)}(0)\right]^{-2}$ ($Z_j = 4.13$, 2.95 and 2.39 for $j = 1$, 2 and 3, respectively). Hence, for $X \ll Y$ (see section 5) we have $\cos^2\theta_j \approx Z_j^{-1}$ and $\theta_j \approx \text{acos}\left(Z_j^{-1/2}\right)$. The values of θ_j obtained with this expression *with the coercive field data*, $\theta_j^{(B)}$, are displayed in table 1. The product of ηM_s^*

can be excluded from equations (8) by taking the ratios of $M_s^{(j)}/M_s^{(i)}$ for $j \neq i$, yielding two equations for θ_j. Solving the system of these equations and equation (6) numerically, we find for $m \gg 1$ the values of θ_j obtained *with the saturation magnetization data*, $\theta_j^{(M)}$, collected in table 1.

It can be seen that both $\theta_j^{(B)}$ and $\theta_j^{(M)}$ satisfy the relation $\theta_1 > \theta_2 > \theta_3$, however differing by ~10–20% for the same direction of the field. These differences between $\theta_j^{(B)}$ and $\theta_j^{(M)}$ cannot be attributed to the influence of the demagnetizing field. Indeed, the relative differences of the demagnetization factors for our samples, estimated using their sizes and equations for a prolate ellipsoid [21, 27], lie between ~2 and 4% yielding negligible corrections to $\theta_j^{(M)}$, while the demagnetization factors for rods are even smaller [29]. Below we show that this disagreement between $\theta_j^{(B)}$ and $\theta_j^{(M)}$ can be explained by a distribution of θ_j around the mean values, which can be taken into account by changing $\theta_j \to \theta_j + \alpha_j$ in equations (6)–(8), where α_j is a random deviation from the mean angle θ_j satisfying the conditions $-\Delta_j < \alpha_j < \Delta_j$ and Δ_j is the width of the distribution of θ_j ($j = 1, 2$ and 3). The distribution function is taken in a stepwise form $f(\alpha_j) = 1/(4\Delta\varphi_j\Delta_j \sin\theta_j)$ for $-\Delta_j < \alpha_j < \Delta_j$ and $f(\alpha_j) = 0$ otherwise, where $\Delta\varphi_j$ is the width of the distribution of the polar angle φ_j around the jth axis. Then the mean value of the magnetization averaged over the above angular distribution, $\langle M_s^{(j)}(0)\rangle = \int M_s^{(j)}(0)\ f(\alpha_j)\,\mathrm{d}\Omega$, satisfies the expression

$$\langle M_s^{(j)}(0)\rangle = C_j \int_{\varphi_j-\Delta\varphi_j}^{\varphi_j+\Delta\varphi_j} \mathrm{d}\varphi_j \int_{-\Delta_j}^{\Delta_j} \mathrm{d}\alpha_j \times [\xi - \lambda\cos^2(\vartheta_j+\alpha_j)]\cos(\vartheta_j+\alpha_j)\sin(\vartheta_j+\alpha_j), \quad (11)$$

where $C_j = \eta M_s^*/(4\Delta\varphi_j\Delta_j\sin\theta_j)$, $\xi = 1 - D_c$ and $\lambda = D_c - D_a$. The integration in equation (11) yields

$$\langle M_s^{(j)}(0)\rangle = \frac{\eta M_s^*}{2\Delta_j}\sin(2\Delta_j)\cos\vartheta_j \times [\xi - \lambda(\cos^2\Delta_j\cos^2\vartheta_j + \sin^2\Delta_j\sin^2\vartheta_j)]. \quad (12)$$

In a similar way we find under the condition of $X \ll Y$ the expression for the mean value of the coercive field,

$$\langle B_c^{(j)}(0)\rangle = \frac{2\pi M_s^* X^{1/2}}{2\Delta_j\sin\vartheta_j}\ln\left(\frac{1+\tan\Delta_j\tan\vartheta_j}{1-\tan\Delta_j\tan\vartheta_j}\right). \quad (13)$$

The widths of the distribution of $\theta_j^{(B)}$ and $\theta_j^{(M)}$, labelled as $\Delta_j^{(B)}$ and $\Delta_j^{(M)}$, respectively, are evaluated by solving the equations for the ratios of $\langle M_s^{(i)}(0)\rangle/\langle M_s^{(k)}(0)\rangle$ and $\langle B_c^{(i)}(0)\rangle/\langle B_c^{(k)}(0)\rangle (i \neq k, i, k = 1, 2$ and 3), respectively, under the condition of equation (6). As can be seen from table 1, the values of Δ_j calculated with the coercivity and the magnetization data are close to each other and lead to overlapping intervals of $\theta_j^{(B)} \pm \Delta_j^{(B)}$ and $\theta_j^{(M)} \pm \Delta_j^{(M)}$. It can also be mentioned that the angular distribution is increased with decreasing θ_j, which is consistent with the expected orientations of the cluster spheroids along or near the growth direction of the ingot.

Finally, we evaluate a set of parameters which depend only weakly on a narrow distribution of the angles and can be calculated by neglecting the scattering of θ_j above. With equations (8), (9) and the expressions $\eta = NV$ and $\mu = M_s^* V$ we find the concentration of the clusters $N = (2\mu)^{-1}G \approx 1.8 \times 10^{14}\ \mathrm{cm}^{-1}$, where $G = \sum_{j=1}^{3} M_s^j(0)/\cos\vartheta_j^{(M)}$ yielding the mean intercluster distance $\langle R\rangle = 2(4\pi N/3)^{-1/3} \approx 240$ nm. Assuming that all or a greatest part of Ni in CdSb enters the $Ni_{1-x}S_x$ nanoclusters we obtain $\eta \approx N_0/N^* \approx 3.8 \times 10^{-3}$, where N^* and N_0 are the concentrations of Ni in $Ni_{1-x}Sb_x$ for $x = 0$ ($N^* = 9.1 \times 10^{22}\ \mathrm{cm}^{-3}$) and in our samples ($N_0 = 3.5 \times 10^{20}\ \mathrm{cm}^{-3}$), respectively. The mean number of Ni ions in a cluster and the mean magnetization of the cluster per Ni are found to be $n \approx N/N^* \approx 1.8 \times 10^6$ and $\mu_{ion} \approx \mu/n \approx 0.01\mu_B$/ion, respectively. Although the values of m and M_s^* could not be determined in our study, useful information can still be obtained taking M_s^* within the limits of ~500–350 emu cm^{-3} corresponding to $x = 0$ and to a minimum value of $x \sim 3.8\%$ for which $T_C > 460$ K, respectively [18, 19]. It can be expected that m is large; however, for the reasons given below (see section 5) we restrict ourselves to values of m between 3 and 15 when some intermediate value of $M_s = 430$ emu cm^{-3} is taken, and with $m = 4$ when using different values of M_s. The mean cluster radius can be obtained with the expression $r = [3M_s^*/(4\pi m\mu)]^{1/3}$. Then the exchange stiffness constant can be evaluated with the formula $A = 2\pi[M_s^*(\kappa/S^2)r/q]^2$ where κ/S^2 can be found with equation (7). Next, equations (4) can be used for evaluations of r_c and r_{sd}, and finally the values of the volume fraction $\eta' = (2M_s)^{-1}G$ and the magnetization per Ni ion in clusters, $\mu'_{ion} = \mu_{ion}\eta/\eta'$, are useful to be calculated for comparison: if all Ni or most part of Ni enters the $Ni_{1-x}Sb_x$ nanoclusters, we should have $\eta \approx \eta'$ and $\mu_{ion} \approx \mu'_{ion}$. In this way we obtain $r \approx 3.1$–2.8 nm, $r_c \approx 1.8$–1.6 nm, $r_{sd} \approx 130$–115 nm, $A \approx (0.5$–$0.8) \times 10^{-6}\ \mathrm{erg\ cm}^{-1}$, $\eta' \approx (0.9$–$0.6) \times 10^{-4}$ and $\mu' \approx 0.4$–$0.6\ \mu_B$/ion for constant $m = 4$ by varying M_s^* within the above limits. On the other hand, for constant $M_s = 430$ emu cm^{-3} and $m = 3$, 4, 6, 8 and 15 we have $r \approx 3.2$, 2.9, 2.5, 2.3 and 1.9 nm, $r_c \approx 2.2$, 1.6, 1.1, 0.7 and 0.4 nm, respectively, and for $m = 3$–15 $r_{sd} \approx 135$–70 nm and $A \approx (1.18$–$0.03) \times 10^{-6}\ \mathrm{erg\ cm}^{-1}$. It can also be obtained with equation (10) that the angles φ_j for $j = 1, 2$ and 3, coincide with $\theta_j^{(M)}$ already at $m \geqslant 4$.

5. Discussion

As mentioned above the picture of blocking in figures 1 and 2, and the field dependence of the blocking temperature (see equation (2) and the upper panel of figure 5), are consistent with the *coherent rotation* of the magnetization of nanosize Ni-rich $Ni_{1-x}Sb_x$ clusters. On the other hand, the anisotropies of the saturation magnetization and the coercivity (figure 4 and the bottom panel of figure 5) give evidence for magnetization reversal by the *curling mode*, in conditions of a narrow distribution of the major axes of the cluster spheroids around a preferred mean direction (table 1). However, there is no contradiction between the interpretations of the magnetization reversal modes. Indeed, estimations at the end of section 4 demonstrate that there is an interval of $4 \leqslant m < 6$–8 where m is high enough to provide all the above approximations (e.g. already at $m = 4$ we have φ_j coinciding with $\theta_j^{(B)}$ and $X/Y \sim 10^{-4}$), r is always much smaller than r_{sd} confirming the strictly single-domain regime and, simultaneously, *r is comparable with r_c*. On the other hand, the broad maximum of $\chi_{ZFC}(T)$ (figure 1) gives evidence for a wide distribution of the sizes of

the clusters around the mean value. Therefore, there should be a wide crossover region between the two magnetization reversal modes which removes the above issue.

As mentioned in section 4 the functions TRM(T), $B_c^{(j)}(T)$ and $M_R^{(j)}(T)$ exhibit two temperature intervals of variation: one with relatively weak dependence on T at high temperatures and the other enhancing when T is decreased (figure 4). The border between these intervals lies near T_b, and therefore such behaviour is consistent with the picture of blocking suggested in section 4. However, the analysis in section 4 is valid only when the interaction between the clusters is not important for blocking. On the other hand, blocking cannot be a reason for enhancement of the low-temperature saturation magnetization. If the majority of Ni enters the nanoclusters we would have quite an opposite picture, a more rapid variation of $M_s^{(j)}(T)$ at high T and slowing down when T is decreased. This issue suggests the presence of a strong paramagnetic (PM) subsystem containing small clusters with small magnetic moments, including probably single Ni ions and remaining unblocked down to 5 K. The PM contribution of the small clusters to the net magnetization is negligible at a high T, but increases to be predominant below ∼100 K. Assuming only nanoclusters we obtain the value of $\mu_{ion} \sim 0.01\ \mu_B$/ion, which cannot exist in the ferromagnetic $Ni_{1-x}Sb_x$ phase having the minimum possible value of ∼0.24 μ_B/ion [18, 19]. It has been demonstrated above that the quantities η and η' do not coincide (see the end of section 4), which is also explained by existence of a great amount of Ni outside the nanoclusters. The fraction of Ni in the nanoclusters can be estimated by the ratio of $\eta/\eta' \sim$ 1.7–2.4% for M_s between 500 and 350 emu cm^{-3}. On the other hand, $\mu'_{ion} = \mu\eta/\eta'$ is between 0.4 and 0.6 μ_B/ion, corresponding to the ferromagnetic phase of $Ni_{1-x}Sb_x$ with x varying from ∼3.8% to 0 and $T_C > 460$ K [18, 19]. Hence, only a small part of Ni in CdSb enters the nanoclusters, while the majority of Ni forms a PM system of even smaller magnetic clusters. At this point, it is reasonable to take for $M_s^{(j)}(0)$ not the values of the saturation magnetization at the smallest T, where the PM contribution is largest, but somewhere inside the temperature interval of a weak variation of $M_s^{(j)}(T)$ where the PM response is negligible, as has been done above (see section 4) in the analysis of the magnetic anisotropy.

Finally we estimate the intercluster interaction energy. The mean distance between the clusters, $\langle R\rangle \approx 240$ nm allows us to exclude the direct exchange interaction between the Ni ions in different clusters. If the PM subsystem in CdSb:Ni contains a minority of single Ni ions and most of them belong to the small clusters (as follows from the activated conductivity of CdSb weakly doped with Ni), then the concentration of the free carriers at the room temperature would be $n_f \sim 10^{15}$ cm^{-3} as typical of undoped CdSb with a moderate degree of compensation [1], which exceeds N by an order of the magnitude. However, n_f decreases exponentially with lowering T down to negligible values near 4.2 K, which corresponds to filling in the acceptor bands of CdSb [1]. This allows us to exclude the long-range RKKY exchange interaction between the clusters mediated by the free carrier spins, because the concentration of the free carriers vanishes rapidly with lowering of T. The dipolar intercluster interaction has a typical energy $W = W_d \approx z_J\mu^2/R^3 \sim 0.1$ meV, where the origin of a constant $z_J \approx 33$ is connected to the long-range character of the dipolar interaction [30]. On the other hand, as can be found from equation (1) using the data in table 1, the anisotropy energy $KV \approx 25kT_b \sim 10^2$ meV exceeds considerably W_d excluding any role of the intercluster interaction in blocking of the cluster moments.

6. Conclusions

We have investigated magnetic properties of oriented CdSb single crystals doped with 2 at% of Ni. Magnetic irreversibility or deviation of the susceptibility data measured for the zero-field-cooled and the field-cooled samples is clearly observed in low fields below 300 K, but vanishes above $B_K \sim 4$ kG which is taken as the anisotropy field of the samples. The zero-field-cooled susceptibility exhibits a broad maximum at T_b, which decreases with increasing the field. The thermoremanent magnetization is observed between 5 and 300 K which deviates considerably from the difference of the field-cooled and the zero-field-cooled magnetizations. Magnetic field dependence of the magnetization displays saturation already above 2–3 T and has a weak temperature dependence between ∼100 and 300 K, which is slightly enhanced below 100 K. In addition, M_s has different values along the crystallographic axes [1 0 0], [0 1 0] and [0 0 1]. The temperature dependence of the coercivity, $B_c(T)$, is weak above T_b and is enhanced below it. The coercive field obeys the relation of $B_c \ll B_K$ and has crystalline anisotropy inverted with respect to that of M_s.

It is concluded that the observed magnetic irreversibility and the anisotropic properties of CdSb:Ni are governed by an assembly of spheroidal Ni-rich $Ni_{1-x}Sb_x$ nanoparticles with a high aspect ratio and broad size distribution. The orientations of these particles are distributed around a preferred direction. The relation $B_c \ll B_K$ and the anisotropies of M_s and B_c are consistent with the magnetization reversal mode by curling, whereas the behaviour of $T_b(B)$ is typical of the coherent rotation mode. This difference can be explained by proximity of the average value of the transversal radius, r, of the clusters to the critical value r_c for transition between the two modes and with the wide crossover interval between these magnetization reversal processes due to the broad distribution of the cluster sizes.

Acknowledgments

This work was supported by the Wihuri Foundation, Finland, and by the Belgorod State University, Russia (grant no. BKG 029-05).

References

[1] Arushanov E K 1986 *Prog. Cryst. Growth Charact* **13** 1
[2] Ashcheulov A A and Gutsul I V 2000 *J. Opt. Technol.* **67** 281
[3] Lazarev V B, Shevchenko V Ya, Grinberg Ya H and Sobolev V V 1978 *Semiconductor Compounds of the II–V Group* (Moscow: Nauka)
[4] Matyas M and Kiegl M 1968 *Czech. J. Phys* **B 18** 356
[5] Andronik I K, Arushanov E K, Emelyanenko O V and Nasledov D N 1968 *Fiz. Tech. Poluprov.* **2** 1248
[6] Cisowski J, Portal J C, Arushanov E K, Broto J M, Huant S and Brunei L C 1984 *Phys. Status Solidi* b **121** 289
[7] Smirnov D V, Mashovets D V, Safonchik M O, Roznovan Yu V and Leotin J 1996 *Semiconductors* **30** 297

[8] Arushanov E K, Cisowski J and Portal J-C 1983 *Proc. 4th All-Union Conf. on Ternary Semiconductors and Their Applications (Kishinev: Shtiintsa)* p 157
[9] Arushanov E K, Lashkul A V, Mashovets D V, Pruglo V I, Radautsan S I and Sologub V V 1982 *Dokl. Akad. Nauk SSSR* **263** 1112
[10] Arushanov E K, Lashkul A V, Lisunov K G, Parfen'ev R V and Radautsan S I 1986 *Sov. Phys. Solid State* **28** 1334
[11] Arushanov E K, Lashkul A V, Lisunov K G, Parfen'ev R V and Radautsan S I 1987 *Sov. Phys. Solid State* **29** 1450
[12] Laiho R, Lashkul A V, Lisunov K G, Lähderanta E, Safonchik M O and Shakhov M A 2004 *J. Phys.: Condens. Matter* **16** 333
[13] Laiho R, Lashkul A V, Lisunov K G, Lähderanta E, Safonchik M O and Shakhov M A 2004 *Semicond. Sci. Technol.* **19** 602
[14] Rarenko I M, Semizorov A F, Slynko V V, Slynko E I and Tovstyuk K D 1974 *Fiz. Electron.* **1** 25
[15] Tovstyuk K D, Slinko E I and Rarenko I M 1969 *Ukr. Fiz. Zh.* **14** 20
[16] Danilevich O I, Ivanchuk R D and Rarenko I M 1975 *Fiz. Electron.* **l0** 38
[17] Marenkin S F, Saidullaeva M, Sanygin V P and Kovaleva I S 1982 *Izv. Akad. Nauk SSSR, Neorg. Mater.* **18** 1759
[18] Hoselitz K 1952 *Ferromagnetic Properties of Metals and Alloys* (Oxford: Clarendon)
[19] Kneller E 1962 *Ferromagnetismus* (Berlin: Springer)
[20] Bean C P and Livingston J D 1959 *J. Appl. Phys.* **30** 120S
[21] Gullity B D 1972 *Introduction to Magnetic Materials* (London: Addison-Wesley)
[22] Wohlfarth E P 1980 *J. Phys. F: Metal Phys.* **10** L 241
[23] Belous N, Zorin I, Kulich N, Lezhnenko I and Tovstolytkin A 1990 *Sov. Phys.—Solid State* **32** 887
[24] Frei E H, Shtrikman S and Trevis D 1957 *Phys. Rev.* **106** 446
[25] Aharoni A 1997 *J. Appl. Phys.* **82** 1281
[26] Sun L, Hao Y, Chien C L and Searson P C 2005 *IBM J. Res. Dev.* **49** 79
[27] Yin H Q and Doyle W D 2002 *J. Appl. Phys.* **91** 7709
[28] Gaunt P 1983 *Philos. Mag.* B **48** 261
[29] Bozorth R M 1956 *Ferromagnetism* (Princeton, NJ: Van Nostrand)
[30] Laiho R, Lisunov K G, Lähderanta E and Zakhvalinskii V S 1999 *J. Phys.: Condens. Matter* **11** 555